AN EXPERIMENTAL INVESTIGATION INTO THE THERMAL MANAGEMENT OF PRISMATIC LITHIUM BATTERY UTILIZING LIQUID-VAPOR PHASE CHANGE COOLING

by

*Wenrui XI, Qiang ZHANG, Ganglin CAO, Lei ZHENG, and Xiongwen ZHANG**

Key Laboratory of Thermal-Fluid Science and Engineering of MOE,
School of Energy & Power Engineering, Xi'an Jiaotong University, Shanxi, China

Integrating a thermal management system for batteries can be a potent means of reducing their operational temperatures. This paper introduces a thermal management system that employs direct contact between the battery and a refrigerant. Through a series of tests examining the battery's cooling performance under conditions of natural convection, passive cooling, and active cooling, a comprehensive evaluation of the battery thermal management system was conducted. Comparing the maximum temperature of the battery at the end of discharge, passive cooling provides reductions of 11.99%, 26.07%, and 32.98% compared to the natural convection at the rate of 1C, 2C, and 3C discharge process, respectively. Furthermore, the effectiveness of active cooling increases as the temperature of the cooling water decreases. There is a temperature drop primarily stemmed from the refrigerant's phase change during the high-rate discharge process. Moreover, the temperature decrease at the moment of phase transition becomes more marked as the ambient temperature rose. In the 3C discharge with 5℃ cooling water circulation, T_{top}, T_{middle}, T_{bottom}, and T_{sides} decreased by 1.63%, 1.90%, 5.21%, and 6.31%, respectively, during the refrigerant phase moment.

Key words: *lithium-ion battery, liquid-vapor phase change, battery thermal management, refrigerant, boiling*

Introduction

With global energy shortage and environmental pollution becoming increasingly prominent, transforming energy consumption, reducing energy risk and reducing carbon emission have become crucial strategies. In the transportation domain, electric vehicles (EV) have garnered extensive recognition due to their elevated energy utilization efficiency and substantial energy-saving potential [1, 2]. Power batteries, essential components of EV, significantly influence their development and adoption, primarily due to their critical role in performance and safety. At this moment, lithium-ion batteries (LIB) reign supreme in the power battery market for electric vehicles, thanks to their higher power density, higher energy density, no memory effect, and lower self-discharge rate, longer calendar and cycle life [3-5].

_____

*Corresponding author, e-mail: xwenz@mail.xjtu.edu.cn

428

Xi, W., *et al.*: An Experimental Investigation Into the Thermal Management …
THERMAL SCIENCE: Year 2025, Vol. 29, No. 1B, pp. 427-439

The LIB generate heat during the charge-discharge cycle due to effects of chemical reaction and internal resistance. The lifespan, safety, and aging rate are concurrently influenced by the operating temperature [6, 7]. Ma *et al.* [5] concluded that the reduction in battery performance primarily results from decreased ionic conductivity and increased charge transfer resistance at low temperatures. Moreover, high temperature conditions accelerate the thermal aging of LIB, potentially shortening their service life. Bandhauer *et al.* [8] illustrated that LIB utilized in electric and hybrid vehicle applications should be kept at temperatures below 50 °C. Additionally, rapid heating (or self-heating within an acceptable cycle) is necessary before operating at low temperatures. Optimal operation for LIB, balancing power capability and aging rate, occurs within the temperature range of 25 °C to 40 °C [9]. Without appropriate thermal management, the temperature of the battery will escalate, thereby adversely impacting its performance and lifespan. Consequently, the investigation and implementation of battery thermal management system (BTMS) have assumed paramount importance [10].

The BTMS can be categorized into three primary types based on their working medium, namely: air cooling, liquid cooling, and phase change cooling [11]. Currently, air cooling and liquid cooling systems for batteries have been introduced in the EV market, while phase change cooling remains in the research and development phase.

Air cooling, as the earliest cooling method, is recognized for its cost-effectiveness, convenience, and high safety [10]. Extensive research has advanced the development of air cooling, and it has found wide applications in the EVs market. Husam *et al.* [12] concluded that optimizing the performance of LIB involves lowering the operating temperature across various air-flow rates. Liquid cooling remains the predominant method of thermal management due to its superior thermal conductivity compared to air [13]. In most cases, liquid cooling utilizes an indirect cooling approach, employing specialized structures with flow channels to exchange heat with the battery. Li *et al.* [14] proposed the overall thermal performance evaluation index parameter to evaluate battery thermal management performance and examined the influences of cooling area and flow direction.

Phase change cooling can be divided into two categories: solid-liquid phase change and liquid-vapor phase change [15]. Typical solid-liquid PCM include paraffin, liquid metal, and expanded graphite, among others. An alternative is cooling through the change of liquid-vapor phase. In comparison to air cooling and liquid cooling, liquid-vapor phase change cooling leverages latent heat to exchange heat with the battery, resulting in higher efficiency. This method allows direct contact between the battery and the refrigerant, leading to improved temperature uniformity. Liquid-vapor phase change cooling surpasses solid-liquid phase change in heat transfer efficiency, making it appropriate for high-capacity batteries, as well as fast charge and discharge scenarios.

Extensive research has focused on the potential utilization of the liquid-vapor phase change in power batteries. Giammichele *et al.* [16] illustrated the feasibility of direct contact between low-boiling-point refrigerants and batteries for cooling purposes. Rahman *et al.* [17] devised an evaporative cooling system for battery temperature control, demonstrating a remarkable 17.69% increase in energy efficiency compared to air-cooled EV. Al-Zareer *et al.* [18] evaluated the cooling performance of an ammonia-boiling thermal management system, highlighting its superior energy efficiency and effectiveness when contrasted with liquid and air cooling systems. Hirano *et al.* [19] immersed batteries discharged at a high rate (20C) in a liquid, effectively maintaining the battery surface temperature at approximately 3 °C. Goodarzi *et al.* [20] developed a thermal management system for an 18650 battery pack using R141-b refrigerant, demonstrating significant cooling quality variations under different liquid immersion heights and discharge rates.

Unfortunately, the existing research on BTM built upon the principles of liquid-vapor phase transition remains lacking in comprehensive coverage. A considerable proportion of researchers have omitted the consideration of pressure effects and have failed to incorporate refrigerant recycling strategies, thereby impeding the ability to evaluate the correlation between refrigerant volume and cooling effectiveness. Moreover, experimental studies focusing on prismatic batteries with high-capacity configurations are notably limited.

In recognition of the deficiencies observed in previous studies, this paper introduces an innovative thermal management system tailored for prismatic LIB, founded on the principles of liquid-vapor phase transition. The key contributions of this research are as: The thermal management system designed in this study operates in a strictly closed state. In the initial state, the battery is maintained in a vacuum. The refrigerant is in direct contact with the battery surface and undergoes recycling within the system to enhance its cooling efficacy. This closed-loop configuration ensures efficient heat dissipation from the battery, emphasizing the integral role of the refrigerant in the cooling process.

Experimental set-up

Experimental system

Figure 1 shows a schematic diagram of the experimental system. This thermal management system required testing under a consistent ambient temperature. A thermostat (GDW-867, NanJing TaiSiTe Testing Equipment Co., LTD) was installed to maintain a constant environment. After the test commenced, the battery generated heat while being supplied with power. A DC power supply (MP6080D, MaiSheng Power Technology Co., LTD) was used to control heating power. Moreover, this system required the injection of circulating cooling water at the top of the test equipment. A thermostatic water tank (MD20-54, KANSA Refrigeration Co., LTD) was installed to supply circulating water. Furthermore, a flow meter was arranged between the thermostatic water tank and test equipment to monitor the mass-flow rate. Finally, the temperature change on the battery surface during the test reflected the cooling effect of this system. A data logger (TP700, ShenZhen Toprie Electronics Co., LTD) was applied to collect temperature data recorded by thermocouples (TT-K-30, Omega, America).
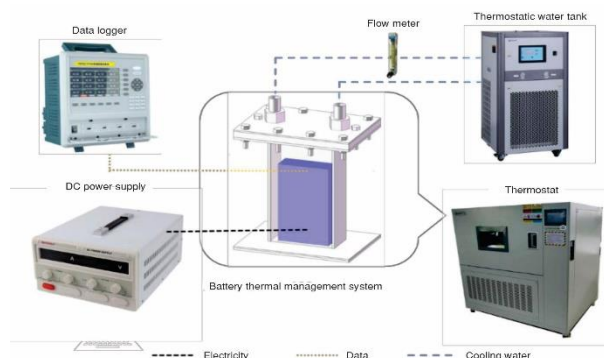

Figure 1. A view of the test set-up

Test section

Figure 2(a) shows the schematic layout of the BTM. The battery was positioned at the central base of the cubic compartment. The side of the battery was 5 mm away from the side

wall of the cubic compartment. Following this placement, a water cooling plate was attached to the upper part of the cubic compartment. The upper part of the battery maintained a distance of 44 mm from the lower surface of the water cooling plate. A groove, measuring 122 mm in length, 80 mm in width, and 7 mm in depth, was machined at the center of the water cooling plate. Ultimately, the upper part of the water cooling plate was connected to both the inlet and outlet of the cooling water. To ensure the device's air tightness, silicone gaskets were placed at the contact surfaces of each component, which were then secured with ten screws.
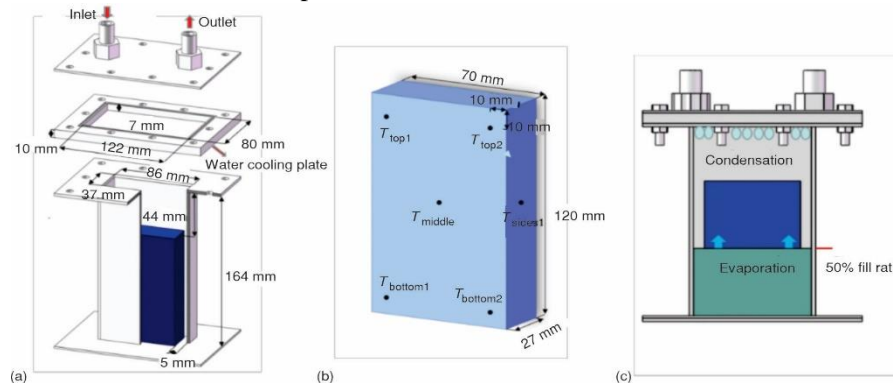

Figure 2. Schematic diagram of BTM; (a) device diagram, (b) thermocouple position on the battery wall surface, and (c) refrigerant circulation process

A 22 Ah prismatic LiNiMnCoO2 (NMC) battery (70 mm × 27 mm × 120 mm in length, width, and height, TianJin LiShen Battery Joint-Stock Co., LTD.) was considered the research subject [21]. The electrolyte material of this battery was gel polymer, and the specific parameters are shown in tab. 1.

Table 1. The 22 Ah prismatic LiNiMnCoO₂ (NMC) battery

Parameters	Units	Values
Rated capacity	Ah	22
Rated voltage	V	3.2
Internal resistance	mΩ	≤1.5
End-of-charge Voltage	V	3.65
End-of-discharge Voltage	V	2.3
Size of battery (length × width × height)	mm	120 × 27 × 70
Pole center distance	mm	40.5
Size of positive and negative electrode (length × width × height)	mm	22 × 7 × 13

However, for safety and various reasons, the battery model in this research was a prismatic aluminum block (117 mm in length, 70 mm in width, and 27 mm in height). To monitor the temperature across various parts of the battery, a total of seven temperature measurement points were positioned, as illustrated in fig. 2(b). Ultimately, a method of averaging was employed to ascertain the temperatures of the four parts:

$$T_{\text{top}} = \frac{T_{\text{top1}} + T_{\text{top2}}}{2} \tag{1}$$

$$T_{\text{middle}} = T_{\text{middle}} \tag{2}$$

$$T_{\text{bottom}} = \frac{T_{\text{bottom1}} + T_{\text{bottom2}}}{2} \tag{3}$$

$$T_{\text{sides}} = \frac{T_{\text{sides1}} + T_{\text{sides2}}}{2} \tag{4}$$

As depicted in fig. 2(c), the aluminum block was in direct contact with the refrigerant within the cubic compartment, requiring the selection of a refrigerant with dielectric properties and a lower boiling point at room temperature. The SF33 was employed as the cooling medium, in which boiling temperature (33.4 °C) is within the optimum operating temperature range (25-40 °C) of LIB. The detailed thermophysical properties of SF33 are listed in tab. 2. The fill ratio of the refrigerant was defined as the ratio of the refrigerant's height to the aluminum block's height. During the test, the heat generated by the battery model prompted the refrigerant to undergo phase conversion from liquid to vapor. The gaseous refrigerant then evaporated and condensed on the underside of the water-cooled plate before returning to the bottom. Assuming that the specific heat capacity and thermal conductivity of the battery remained constant and the battery was simplified as a prism, the transient heat transfer of the battery adhered to the energy conservation equation [21]:

$$\rho_{\text{LIB}} c_{\text{LIB}} \frac{\partial T}{\partial t} = \lambda_x \frac{\partial^2 T}{\partial^2 x} + \lambda_y \frac{\partial^2 T}{\partial^2 y} + \lambda_z \frac{\partial^2 T}{\partial^2 z} + Q_{\text{LIB}} \tag{5}$$

In this paper, Euler model was used to describe the gas-liquid flow process of SF33 in LIB cooling system. The model mainly included mass conservation equation, momentum conservation equation, and energy conservation equation of two-phase mixture, which were expressed in the rectangular coordinate system as:

– The mass conservation equation was

$$\frac{\partial \rho_m}{\partial t} + \nabla(\rho_m U_m) = 0 \tag{6}$$

– The momentum conservation equation was

$$\frac{\partial}{\partial t} \sum_{k=l,v} (\rho_k U_k) + \nabla \sum_{k=l,v} \{\rho_k U_k \otimes U_k\} = -\nabla p + \nabla \tau_{\text{eff},m} \tag{7}$$

– The energy conservation equation was

$$\frac{\partial}{\partial t} \sum_{k=l,v} (\alpha_k \rho_k E_k) + \nabla \sum_{k=l,v} \left[\alpha_k U_k (\rho_k E_k + p) \right] = \nabla \left(k_{\text{eff},m} \nabla T + U_m \tau_{\text{eff},m} \right) + S_E \tag{8}$$

where ρ_m is the mass of the mixture, U_m – the velocity of the mixture, α_k – the vapor volume fraction, ρ_k – the density of the k phase, and U_k – the velocity of the k phase. The angular labels l and v, respectively, represented SF33 liquid and SF33 steam, $\tau_{\text{eff},m}$ stood for the effective shear stress tensor, E_k – the total energy of the k phase, P – the pressure, $k_{\text{eff},m}$ – the effective thermal conductivity of the SF33 two-phase mixture, and S_E – the source term, representing the external energy entering the system. In this article, it referred to the heat generated by LIB.

Experimental conditions

The phase of the experiment entailed the monitoring of temperature fluctuations during discharge under a natural convection state, passive cooling state, and active cooling state.

Under the natural convection state, the aluminum block was introduced into the open cubic compartment, enabling efficient heat exchange between the aluminum block and the surrounding air. Filling the refrigerant in the sealed cubic compartment without water circulation on the upper surface of the water cooling plate is referred to as passive cooling. This active cooling system was built upon passive cooling by introducing circulating cooling water to enhance the cooling efficiency of the water cooling plate.

Table 2. The SF33 parameters [22]

Parameters	Units	Values
Chemical structure Molecular weight	$gmol^{-1}$	Cis-CF_3CH–CHCF$_3$ 164
Boiling point	°C	33.4
Freezing point	°C	-107
Density at 25 °C	gcm^{-3}	1.36
Viscosity at 25 °C	Pa·s	0.38
Resistivity	ohm·cm^{-1}	10^8
Break down voltage	kV	10
Heat of vaporization	$kJkg^{-1}$	166
Liquid specific heat at 25 °C	$kJkg^{-1}K^{-1}$	1.2

The discharge rate was defined as the current value required for the battery to discharge its rated capacity within a specified period, which was numerically equal to the number of times the rated capacity of the battery. It was defined as:

$$C - Rate = \frac{I}{C} \tag{9}$$

where I is the discharge current, C-$Rate$ – the discharge rate, and C – the rated capacity. Each group of experiments was conducted by changing the discharge rate (1C, 2C, and 3C) and ambient temperature (25 °C and 35 °C), which was controlled by the thermostat. Especially, experiments of active cooling were conducted by changing the temperature (5 °C, 15 °C, 25 °C) of circulating water. Circulating cooling water flow was set to 20 Lph. The initial power for the aluminum block at different discharge rates was determined according to the experimental result of battery heat generation by Zhang *et al.* [21]. The discharge times of 1C, 2C, and 3C were found to be 3940 seconds, 2020 seconds, and 1340 seconds. Additionally, the maximum temperature of the aluminum block exhibited an almost linear increase with the discharge times. The heating powers of the battery monomer were 2.68 W, 8.31 W, and 16.96 W.

Experimental uncertainty

As previously stated, temperatures of the aluminum block were measured by *K*-type thermocouples, which also were acquired by the data logger. The power of heating the

Table 3. Accuracies of main devices

Parameters	Units	Accuracy
T (K-type)	°C	±0.5
T (data logger)	°C	±0.2
P (DC power supply)	W	±1%
Mass-flow rate (flow meter)	Lph	±0.2%
P (pressure sensor)	kPa	±1%

aluminum block was supplied by the DC power supply. The mass-flow rate was measured by the flow meter. Table 3 summarizes the accuracies of the main devices. In this research, all these quantities were measured parameters, and the uncertainties were only related to the accuracies of individual measurement devices.

According to the Schulz and Cole method, the standard error Δy of y can be calculated as [23]:

$$y = f\left(x_1, x_2, x_3, \ldots, x_n\right) \tag{10}$$

$$\Delta y = \left[\left(\frac{\partial y}{\partial x_1}\Delta x_1\right) + \left(\frac{\partial y}{\partial x_2}\Delta x_2\right) + \left(\frac{\partial y}{\partial x_3}\Delta x_3\right) + \ldots + \left(\frac{\partial y}{\partial x_n}\Delta x_n\right)\right]^{1/2} \tag{11}$$

where y is a function of x, Δx_1, Δx_2, $\Delta x_3, \ldots, \Delta x_n$ denote the measurement error. The accuracies of the K-type thermocouple and the data logger are ± 0.5 °C and ± 0.2 °C, respectively, the resulting errors for T and ΔT will be ± 0.54 °C and ± 0.76 °C.

Result and discussion

The experimentation followed a sequential approach: firstly, the battery's discharge process at different rates was simulated under natural convection, revealing the temperature fluctuations on the battery surface without the integration of a BTM. Subsequently, the 50% fill ratio, F_r, was tested, with no circulating cooling water passing through the water cooling plate's surface, defining this setup as passive cooling. The cooling effectiveness of passive cooling was then compared to that of natural cooling. Lastly, building upon passive cooling, circulating cooling water was introduced at different temperatures, T_w, to assess its impact on cooling performance.

Natural cooling

Figure 3 illustrates the temperature distribution on the battery's surface at discharge rates of 1C, 2C, and 3C, with an ambient temperature of 25 °C under natural convection. When the battery was discharging at 2C, the maximum surface temperature reached 44.6 °C at the end of the discharge process. The maximum temperature reached 56.4 °C for the discharge rate of 3C. It must be emphasized that the maximum temperature recorded on the battery surface after the 2C or 3C discharge exceeded the prescribed safety temperature range [9].

Besides focusing on the highest temperature, the surface temperature difference was also a crucial research parameter. Using the 3C discharge process as an example, the T_{middle} reached 56.4 °C, while the T_{top}, T_{bottom}, and T_{sides} reached 56.3 °C, 56 °C, and 55.6 °C, respectively, with a maximum temperature difference of 0.8 °C between each part. In sum, the temperature distribution across the battery's surface under natural convection remained highly uniform, with temperature differentials not exceeding 1°C throughout the entire discharge process. Zhang [24] *et al.* thought that maintaining a temperature distribution with a temperature difference of less than 5 °C was desirable to mitigate non-uniform chemical reactions within the battery.

Passive cooling

Passive cooling proved more energy-efficient than active cooling, achieving a certain degree of cooling effect without the need for pump power consumption. The temperature difference between passive cooling ($T_a = 25$ °C and $F_r = 50\%$) and natural convection ($T_a = 25$ °C) is shown in fig. 4. At the end of the 1C discharge, the highest temperature recorded on various

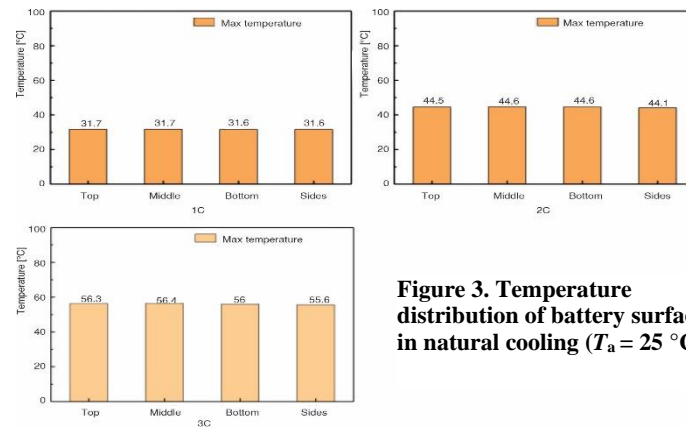**Figure 3. Temperature distribution of battery surface in natural cooling ($T_a = 25$ °C)**

parts of the battery under natural convection reached 31.7 °C, whereas, under passive cooling, the maximum temperature was 28.3 °C. The maximum temperature showed a notable reduction of 11.99%. Notably, the internal pressure of the cubic compartment at the onset of the 1C discharge rate was –14.8 kPa, with the boiling point of the refrigerant SF33 recorded at 29.1 °C at this pressure. The compartment's pressure increased in tandem with the battery's temperature. While the boiling point of the refrigerant also rose with the battery's temperature, it did not exceed 29.1 °C at the end of the discharge process. Consequently, we concluded that when the temperature curve during discharge exhibited inconspicuous fluctuation, the battery primarily relied on the sensible heat of the refrigerant for heat dissipation. Even in the absence of a phase change, the liquid refrigerant SF33 exhibited superior thermal conductivity compared to air, leading to more efficient cooling than natural convection.
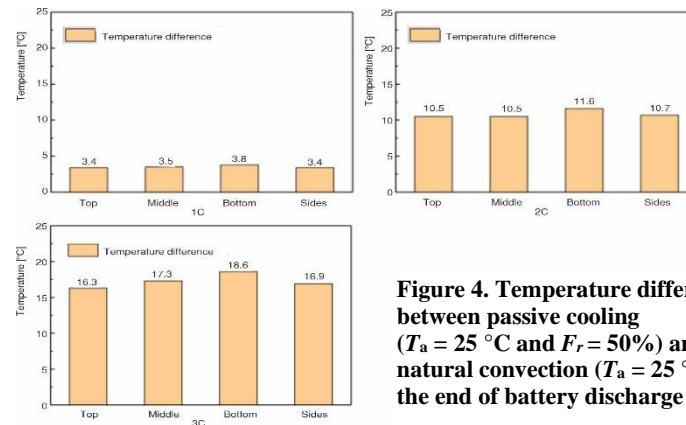

Figure 4. Temperature difference between passive cooling ($T_a = 25$ °C and $F_r = 50$%) and natural convection ($T_a = 25$ °C) at the end of battery discharge

At the end of the 2C and 3C discharge processes, the maximum temperatures observed on various parts of the battery surface with passive cooling exhibited reductions of 26.07% and 32.98%, respectively, compared to natural cooling. Clearly, at higher discharge rates, the refrigerant was more likely to undergo phase change. The cooling effect generated by this phase change was more ideal. Kim *et al.* [10] argued that the refrigerant phase transition offered superior cooling efficacy for the battery at high rates compared to alternative cooling methods. Therefore, the SF33 immersion cooling scheme was capable of efficiently absorbing the substantial heat generated by the battery during high rates of discharge, thereby maintaining the battery temperature within the optimal temperature range.

Active cooling

      The passive cooling approach employing SF33 immersion ensured minimal temperature fluctuations during the dynamic operation of LIB, even in unpredictable real-world scenarios [25]. However, to investigate the impact of the condensation rate of the refrigerant in the phase change cycle on BTM effectiveness, it was of research significance to employ active cooling with varying temperature gradients in the cooling water. Figure 5 illustrates temperature variations across different sections of the battery as circulating coolant water with varied temperatures is introduced at a 50% fill ratio and 25 °C ambient temperature. Throughout the discharge at the 3C rate with 25 °C circulating cooling water, the battery surface's top, middle, bottom, and sides experienced a decrease over 1056 seconds, 1043 seconds, 1033 seconds, and 1046 seconds. These instances indicated that the battery's surface temperature neared the boiling point of the coolant at the current pressure. The abrupt temperature changes signified a phase transition in the refrigerant, absorbing heat from the battery and causing a temperature reduction. However, the timing of this temperature decline did not exhibit a clear correlation with the T_w. The pressure within the cubic compartment significantly influenced the refrigerant's boiling point. The escalation in battery temperatures increased the cubic compartment's pressure, subsequently raising the boiling point of the refrigerant. Consequently, the temperature decrease on the battery surface during the 3C discharge primarily stemmed from the refrigerant's phase change, a phenomenon absented during discharge processes at 1C and 2C rates.
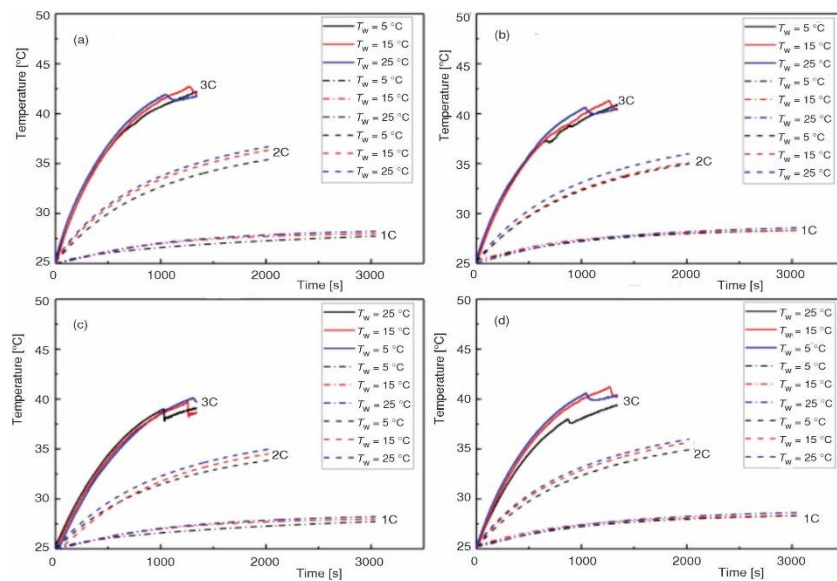

**Figure 5. Influence of T_w on the heat dissipation effect of;
(a) top, (b) middle, (c) bottom, and (d) sides of the battery
($T_a = 25$ °C and $F_r = 50\%$)**

      Throughout the 1C and 2C discharge processes, the battery's surface temperature consistently increased without fluctuation, implying that the boiling process did not happen. The lower part of the battery depended on the sensible heat of the refrigerant for heat dissipation, while the upper part of the battery lacked direct contact with the refrigerant. With 25 °C cooling water, the maximum temperatures for each part following the 2C discharge process were as follows: the T_{top}, T_{middle}, T_{bottom}, and T_{sides} reached 36.6 °C, 34.9 °C, 34.8 °C, and 35.8 °C,

respectively. Particularly, the upper part of the battery, without refrigerant contact, maintained a higher temperature than other parts. These temperature patterns remained consistent, irrespective of whether T_w was set at 5 °C or 15 °C.

As shown in fig. 6, when the power was lowered at 1C and 2C, the maximum temperature of the battery surface was positively correlated with the temperature of the cooling water, because the battery relies on sensible heat of the refrigerant to dissipate heat, and the temperature of the cooling water played a decisive role in the cooling effect. However, when the power was lowered at 3C, the temperature of the cooling water affected the boiling point of the refrigerant phase transition, resulting in different phase transition times of the refrigerant around the battery at different cooling water temperatures. Therefore, there was no positive correlation between the maximum temperature of the battery surface and the temperature of the cooling water.
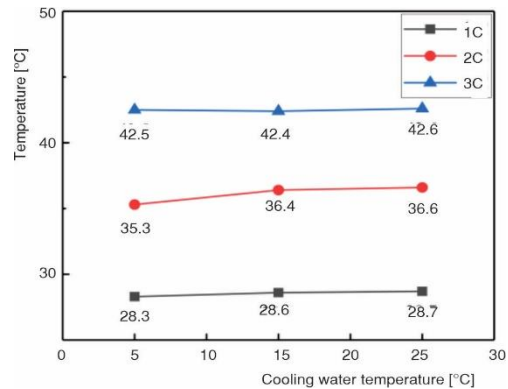

Figure 6. Effect of different cooling water temperature on maximum temperature

In summary, utilizing the refrigerant's sensible heat for battery heat dissipation yielded suboptimal results. However, although active cooling is more beneficial for battery cooling, a more detailed examination is required to assess the balance and optimization between the power consumption and energy equilibrium of the cooling water.

Effect of ambient temperature

Elevated external ambient temperature was a crucial factor constraining the high-performance operation of EV power battery. Excessive ambient heat can result in heightened impedance and expedited capacity degradation in LIB. Simultaneously, lower ambient temperatures impeded the chemical reactions within the battery, slowing down the discharge process [26, 27]. The BTM was significantly relied on the ambient temperature. As the ambient temperature increased, there was a notable increase in both the pressure within the cubic compartment. Hence, investigating the impact of extreme ambient temperatures on BTM hold practical significance. Figure 7 demonstrates temperature variations across different parts of the battery as circulating coolant water, with varying temperatures, was introduced at a 50% fill ratio and 35 °C ambient temperature. No discernible temperature fluctuations were observed in any area during the 1C discharge. In the 2C discharge process, the maximum temperature in each part of the battery increased by less than 5 °C, and no abrupt temperature changes occurred. With the rise in battery temperature, the pressure inside the cubic compartment also increased. This resulted in an increase in the boiling point of the refrigerant due to the heightened pressure, indicating that the heat generated by the battery during the 2C discharge was inadequate to reach the refrigerant's boiling point.

The increase in ambient temperature significantly influenced temperature fluctuations during high-rate battery discharges. Under the 3C discharge rate, all regions of the battery surface encountered a sudden temperature drop, succeeded by a gradual increase. Particularly, the temperature disparity between the lower end and sides of the battery was more evident, signifying a more prominent temperature decrease in areas directly contact with the refrigerant. With an ambient temperature of 35 °C, the post-drop temperature difference became more apparent,
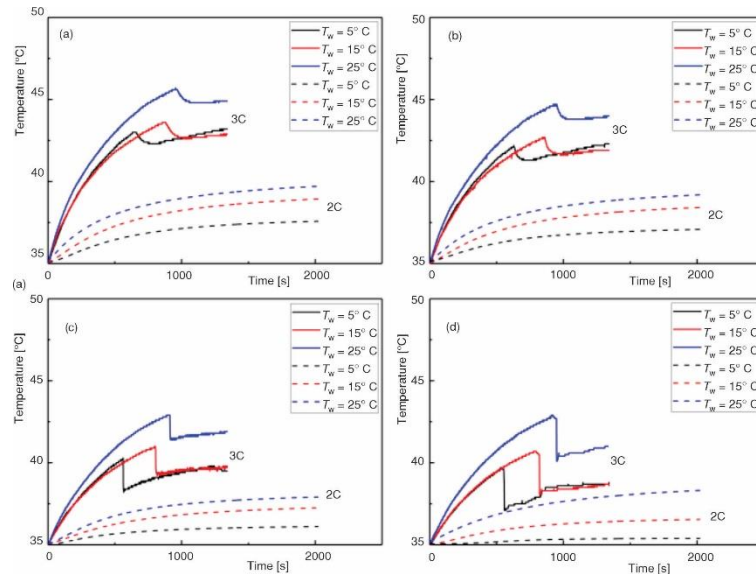
**Figure 7. Influence of T_w on the heat dissipation effect of;
(a) top, (b) middle, (c) bottom, and (d) sides of the battery
($T_a = 35$ °C and $F_r = 50\%$)**

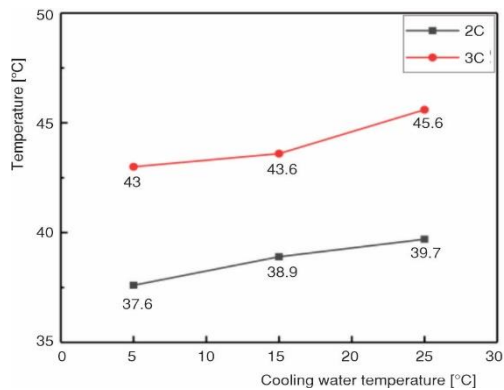**Figure 8. Effect of different cooling water
temperature on maximum temperature**

indicating the increased effectiveness of this thermal management system at higher temperatures. In the 3C discharge with 5 °C cooling water circulation, the complete discharge process took 1340 seconds to finish. Figure 8 presents the surface temperatures of the battery at the onset and conclusion of the refrigerant phase transition. During the refrigerant phase moment, T_{top}, T_{middle}, T_{bottom}, and T_{sides} decreased by 1.63%, 1.90%, 5.21%, and 6.31%, respectively.

As shown in fig. 8, when the battery was discharged at 2C and 3C, the maximum surface temperature was positively correlated with the cooling water temperature, and the gradient change at high temperature was greater than that at 25 °C, and the influence of cooling water temperature at high temperature was greater than that at normal temperature.

The process of refrigerant changing from liquid to vapor involved absorbing heat to overcome molecular attraction. In a vacuum, devoid of an external heat source, the refrigerant absorbed heat generated by the battery, leading to a rapid temperature decrease. It was crucial to recognize that, when all the liquid had converted to vapor, supplying additional heat would still elevate the temperature of the battery. In low pressure environments, liquid molecules can more readily transition from liquid to vapor, necessitating energy absorption, and thus causing a temperature drop. In summary, changes in ambient temperature minimally impacted temperature fluctuations on the battery surface during low-rate discharge. The cooling effectiveness achieved through refrigerant phase change was notably remarkable when the battery was discharged at the 3C rate following an elevation of the ambient temperature to 35 °C.

438

Xi, W., *et al.*: An Experimental Investigation Into the Thermal Management …
THERMAL SCIENCE: Year 2025, Vol. 29, No. 1B, pp. 427-439

Conclusions

This study experimentally examined the heat dissipation of a prismatic LIBS using a thermal management system with liquid-vapor phase change. The study examined the influence of several factors, such as ambient temperature and circulating cooling water temperature, on the temperature increase of the battery. It can be inferred that the following conclusions can be drawn.

- The BTMS with passive cooling had a certain degree of effect on battery heat dissipation. Comparing the maximum temperature of the battery at the end of discharge, passive cooling provided reductions of 11.99%, 26.07%, and 32.98% compared to the natural convection at the rate of 1C, 2C, and 3C discharge process, respectively. The maximum temperature of the battery surface can be effectively reduced using the BTMS with active cooling. The cooling quality of the battery improved with decreasing temperature of the circulating cooling water.
- The cooling quality of the battery was more pronounced during high-rate discharge and 35 °C ambient temperature. Especially, there was a temperature drop primarily stemmed from the refrigerant's phase change during the high-rate discharge process. In the 3C discharge with 5 °C cooling water circulation, T_{top}, T_{middle}, T_{bottom}, and T_{sides} decreased by 1.63%, 1.90%, 5.21%, and 6.31%, respectively during the refrigerant phase moment.

Acknowledgment

Nomenclature

F_r – fill ratio, [%]
T – temperature, [°C]

Subscripts

a   – ambient
bottom – bottom of the battery
middle – middle of the battery
r   – refrigerant

sides   – sides of the battery
top   – top of the battery
w   cooling water

Acronyms

EV   electric vehicles
LIB   lithium-ion batteries
BTMS   battery thermal management system

References

[1] Amjad, S., *et al.*, Review of Design Considerations and Technological Challenges for Successful Development and Deployment of Plug-in Hybrid Electric Vehicles, *Renewable and Sustainable Energy Reviews*, *14* (2010), 3, pp. 1104-1110
[2] Ahmadi, P., Environmental Impacts and Behavioral Drivers of Deep Decarbonization for Transportation Through Electric Vehicles, *Journal of Cleaner Production*, *225* (2019), July, pp. 1209-1219
[3] Speirs, J., *et al.*, The Future of Lithium Availability for Electric Vehicle Batteries, *Renewable & Sustainable Energy Reviews*, *35* (2014), July, pp. 183-193
[4] Etacheri, V., *et al.*, Challenges in the Development of Advanced Li-Ion Batteries: A Review, *Energy & Environmental Science*, *4* (2011), 9, pp. 3243-3262
[5] Ma, S., *et al.*, Temperature Effect and Thermal Impact in Lithium-Ion Batteries: A Review, *Progress in Natural Science-Materials International*, *28* (2018), 6, pp. 653-666
[6] Barre, A., *et al.*, A Review on Lithium-Ion Battery Ageing Mechanisms and Estimations for Automotive Applications, *Journal of Power Sources*, *241* (2013), Nov., pp. 680-689

[7] Doughty, D., Roth, E. P., A General Discussion of Li-Ion Battery Safety, *Electrochemical Society Inter-face*, *21*. (2012), 2, pp. 29-36
[8] Bandhauer, T. M., *et al.*, A Critical Review of Thermal Issues in Lithium-Ion Batteries, *Journal of The Electrochemical Society*, *158*. (2011), 3, p. R1
[9] Zhang, J. Y., *et al.*, Advanced Thermal Management System Driven by Phase Change Materials for Power Lithium-Ion Batteries: A Review, *Renewable & Sustainable Energy Reviews*, *159* (2022), 112207
[10] Kim, J., *et al.*, Review on Battery Thermal Management System for Electric Vehicles, *Applied Thermal Engineering*, *149* (2019), Feb., pp. 192-212
[11] Bhattacharjee, A., *et al.*, Design of an Optimized Thermal Management System for Li-Ion Batteries under Different Discharging Conditions, *Energies*, *13* (2020), 21, 5965
[12] Hasan, H. A., *et al.*, A Novel Air-Cooled Li-Ion Battery (LIB) Array Thermal Management System - A Numerical Analysis, *International Journal of Thermal Sciences*, *190* (2023), 108327
[13] Wu, W. X., *et al.*, A Critical Review of Battery Thermal Performance and Liquid Based Battery Thermal Management, *Energy Conversion and Management*, *182* (2019), Feb., pp. 262-281
[14] Li, M., *et al.*, Performance Analysis of Liquid Cooling Battery Thermal Management System in Different Cooling Cases, *Journal of Energy Storage*, *72* (2023), 108651
[15] Jaguemont, J., Van Mierlo, J., A Comprehensive Review of Future Thermal Management Systems for Battery-Electrified Vehicles, *Journal of Energy Storage*, *31* (2020), 101551
[16] Giammichele, L., *et al.*, Experimental Study of a Direct Immersion Liquid Cooling of a Li-Ion Battery for Electric Vehicles Applications, *International Journal of Heat and Technology*, *40* (2022), 1, pp. 1-8
[17] Rahman, A., *et al.*, Fuzzy Controlled Evaporative Battery Thermal Management System for EV/HEV, *International Journal of Electric and Hybrid Vehicles*, *7* (2015), 1, pp. 22-39
[18] Al-Zareer, M., *et al.*, Development and Evaluation of a New Ammonia Boiling Based Battery Thermal Management System, *Electrochimica Acta*, *280* (2018), Aug., pp. 340-352
[19] Hirano, H., *et al.*, Boiling Liquid Battery Cooling for Electric Vehicle, *Proceedings*, IEEE Transportation Electrification Conference and Expo, Asia-Pacific (ITEC Asia-Pacific), Beijing, China, 2014
[20] Goodarzi, M., *et al.*, Experimental Study of Li-Ion Battery Thermal Management Based on the Liquid-Vapor Phase Change in Direct Contact with the Cells, *Journal of Energy Storage*, *62* (2023), 106834
[21] Zhang, Q., *et al.*, Study of Wet Cooling Flat Heat Pipe for Battery Thermal Management Application, *Applied Thermal Engineering*, *219* (2023), 119407
[22] Li, Y., *et al.*, Experimental Studies of Liquid Immersion Cooling for 18650 Lithium-Ion Battery Under Different Discharging Conditions, *Case Studies in Thermal Engineering*, *34* (2022), 102034
[23] Liang, L., *et al.*, Inclined U-Shaped Flat Microheat Pipe Array Configuration for Cooling and Heating Lithium-Ion Battery Modules in Electric Vehicles, *Energy*, *235* (2021), 121433
[24] Zhang, J., *et al.*, Advanced Thermal Management System Driven by Phase Change Materials for Power Lithium-Ion Batteries: A Review, *Renewable and Sustainable Energy Reviews*, *159*. (2022), 112207
[25] Li, Y., *et al.*, Experimental Studies of Liquid Immersion Cooling for 18650 Lithium-Ion Battery Under Different Discharging Conditions, *Case Studies in Thermal Engineering*, *34* (2022), 102034
[26] Liang, J. L., *et al.*, Investigation on the Thermal Performance of a Battery Thermal Management System Using Heat Pipe Under Different Ambient Temperatures, *Energy Conversion and Management*, *155* (2018), Jan., pp. 1-9
[27] Kong, D.P., *et al.*, A Novel Battery Thermal Management System Coupling with PCM and Optimized Controllable Liquid Cooling for Different Ambient Temperatures, *Energy Conversion and Management*, *204* (2020), 11228